THE INFLUENCE OF IN-PLANE ROUGHNESS WAVELENGTH RELATIVE TO THE TURBULENT BOUNDARY LAYER THICKNESS

***B. Nugroho*[1], *I.K.A.P. Utama*[2], *J.P. Monty*[1], *N. Hutchins*[1], *and B. Ganapathisubramani*[3]**

[1] ***The University of Melbourne, Australia***
[2] ***Institut Teknologi Sepuluh Nopember, Indonesia***
[3] ***The University of Southampton, United Kingdom***

bagus.nugroho@unimelb.edu.au

Abstract

A naturally formed roughness from a recently cleaned and painted ship hull was scanned, scaled and replicated for laboratory testing to systematically investigate the ratio of in-plane roughness wavelength, λ, with respect to the boundary layer thickness δ. Experiments were conducted by varying the roughness average height k_a^+ and in-plane roughness wavelength λ via simple geometric scaling while maintaining a constant effective slope ES_x (defined as the average streamwise gradient of the roughness). For this study, we scale the scanned roughness topography by a factor of 2.5 and 15, and measure the mean velocity profiles in the turbulent boundary layers developing over these surfaces at a range of Reynolds number. The results indicate that the $2.5\times$ scaled roughness behaves like a traditional sand grain or 'k-type' roughness, while the $15\times$ does not. It seems that the $15\times$ scaled roughness generates a large scale spanwise velocity variation that extends to the logarithmic region, causing a break in outer layer similarity. Surprisingly, at the highest Reynolds numbers, the $2.5\times$ surface has a larger roughness function ΔU^+ (and hence drag coefficient) than the $15\times$, even though it has a physically smaller roughness height. We believe that this curious result occurs because the $15\times$ surface has in-plane lengthscales λ that approach the boundary layer thickness.

1 Introduction

In the last eight decades, the study of wall-bounded turbulent flow over rough surfaces has received considerable attention due to its importance in various engineering applications. These include boundary layers over ship hulls (Monty *et al* 2016) and pipe flow (Moody 1944). Rough wall turbulent boundary layers are an important topic, as the roughness is known to generate a higher wall drag than that of a smooth wall. This increase in drag manifests as a downward shift of the viscous scaled streamwise mean velocity profile in the logarithmic region, known as the Hama (1954) roughness function, $\Delta U^+ = \Delta U/U_\tau$. Here U is streamwise mean velocity, U_τ is skin friction velocity given by $U_\tau = \sqrt{\tau_w/\rho}$, where τ_w is wall shear stress, and ρ is fluid density. The magnitude of this shift is proportional to the increase in wall drag due to the roughness, and is a measure of the effect of a given surface roughness on the flow. We usually characterise this shift in terms of an equivalent sandgrain roughness k_s, which though measured in meters, is not a directly observable quantity of the roughness topography, but rather a measure of this fluid effect. The lengthscale k_s is strictly speaking the size of a close-packed uniform sandgrain roughness from the experiments of Nikuradse (1933) which would have the same effect on the flow as the observed surface topography.

A major challenge in the study of flow over a rough surfaces is the wide range of roughness properties that can contribute to the flow dynamics, and hence k_s and the drag penalty. Solidity, effective slope, average roughness height, skewness, etc. have all been investigated (see Flack and Schultz (2010) for a recent review). An important concept in the study of turbulent boundary layer over a rough surface is the assumption of Townsend's (1976) outer layer similarity hypothesis. The hypothesis states that above the roughness sublayer, turbulent motions are independent of the surface roughness and viscosity at a sufficiently large Reynolds number. The existence of outer layer similarity can be identified from the collapse of mean velocity defect and outer-scaled turbulence intensity profiles between the rough surface and smooth surface (see Flack and Schultz (2010) and Monty *et al* 2016). Strictly speaking, outer layer similarity is only expected when the roughness lengthscale is small compared to the boundary layer thickness (Townsend 1976). Researchers usually interpret this as a requirement that the ratio k/δ must be small (Jiménez 2004). However, for the experiments conducted here, we will look at cases where k/δ remains marginal, yet the ratio of in-plane roughness wavelength to boundary layer

thickness λ/δ becomes large. Such scenarios are possible with surfaces that have quite low solidities or effective slopes.

A recent study by Napoli *et al* (2008) reveals that effective slope ES_x is an important roughness property. This study indicates that for their particular range of rough surfaces investigated, ΔU^+ scales relatively well with ES_x, irrespective of viscous scaled roughness height. On the other hand, experimental results from Schultz and Flack (2009) show that for large ES_x (i.e > 0.35) ΔU^+ is more strongly dependant on the roughness height rather than ES_x. Following the study of Napoli *et al.* (2008) and Schultz and Flack (2009), a more recent report by Chan *et al.* (2015) shows that roughness function ΔU^+ indeed depends on both effective slope ES_x and a scale of roughness height (in this case the roughness height was characterised with the viscous scaled average roughness height k_a^+). For this report, we will investigate the ratio of in-plane roughness wavelength, λ, to the boundary layer thickness δ. We will conduct this experimentally by varying k_a^+ and λ through a simple geometric scaling of the rough surface, while maintaining a constant effective slope ES_x.

2 Experiment Methods

Surface Roughness Scanning and Manufacturing

For this study, a rough surface from a recently cleaned and painted ship hull is recorded during drydock via imprint using silicone rubber. The imprint is then scanned using a Keyence^{TM} LK-031 laser triangulation sensor that is attached to a two-axis computer controlled positioning system. Figure 1 illustrates the resulting scan over a 50×50 mm surface area and table 1 shows the key surface roughness parameters. The roughness pattern has a distinct orange-peel texture with an in-plane roughness wavelength, $\lambda = 1.12$ mm, obtained via autocorrelation with a threshold of 0.1, following Acharya *et al*. (1986).

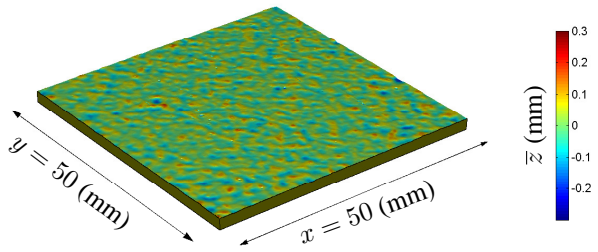

Figure 1: Ship hull surface roughness scan.

The digital roughness data is then scaled and manufactured for measurements in a relatively low Reynolds number wind tunnel. Here two different geometrically scaled surfaces, namely 2.5 and 15 times, are scaled. The geometric scaling results in the increase of λ and k_a, however, the ES_x (and hence solidity) value remains unchanged. The scaled roughness is then modified in such a way that the surface is

Parameter	Value	Units	Formula
k_a	0.0413	mm	$\overline{\lvert z' \rvert}$
k_{rms}	0.0519	mm	$\sqrt{\overline{z'^2}}$
k_p	0.4791	mm	max z' - min z'
k_{sk}	0.0868	-	$\overline{z'^3/k_{rms}^3}$
k_{ku}	3.0712	-	$\overline{z'^4/k_{rms}^4}$
ES_x	0.0890	-	$\overline{\lvert dz'/dx \rvert}$

Table 1: Key surface roughness parameters from the laser scanning, where z' is the surface deviation about the mean height ($z' = z - \overline{z}$)

periodic or tesselates in both streamwise and spanwise directions. The surface roughness is manufactured using a three-axis CNC machine to create a master tile with a surface area of 505 x 285 mm and replicated via moulding and casting techniques. In total 27 of these replicated tiles are used to form the test surface. The manufacturing method is similar to that of Nugroho *et al.* (2013), Monty *et al.* (2016) and Kevin (2016).

Measurement Technique

The measurements are conducted in an open-return blower-type boundary layer wind tunnel with a contraction ratio of 8.9:1. The tunnel has a working section with cross-sectional dimensions of 0.94 $\times$ 0.375 m (width $\times$ height) and length 6.7 m. The resulting surface roughness is laid inside the tunnel, covering the entire 6.7 $\times$ 0.94 m^2 surface area. The flow measurements for both roughness sizes (2.5 and 15 times scaled) and for the smooth-wall reference are performed at zero pressure gradient (ZPG) conditions using single-normal boundary layer type hot-wire sensors over a range of free stream velocities (10 m/s, 15 m/s, 20 m/s and 25 m/s). The hot-wire probe is operated using an in-house designed Melbourne University Constant Temperature Anemometer (MUCTA). The sensing element of the hot-wire is Platinum Wollaston wire with 5 µm diameter. The hot-wire is etched to length 1 mm, resulting in a length-to-diameter ratio of 200 to minimise end conduction (Ligrani and Bradshaw 1987). It should be noted that as the freestream velocity (and hence the friction velocity) increases, so will the viscous scaled wire length l^+, which will result in an increasing attenuation of small-scale fluctuations (Hutchins *et al*. 2009).

In this study all measurements are conducted at the same streamwise location $x = 4$ m downstream of the tunnel inlet (see table 2 for key flow parameters). The hot wire probe is mounted to a two-dimensional traverse fitted with encoders, allowing accurately spanwise and wall-normal positioning. For the smooth-wall reference case, the hot-wire measures the mean streamwise velocity profile at 50 logarithmically-spaced measurement stations in the wall-normal direction covering 150 mm height ($\approx 3\delta$). For the rough wall cases (both the 2.5 and 15 times scaled), measurements are made over a spanwise and wall-normal plane (30 points in the wall normal direc-

Wall type	U_∞ (m/s)	x (m)	k_a (mm)	δ/k_a	ES_x	λ (mm)	δ/λ	δ (m)	U_τ (m/s)	Re_τ	ΔU^+	l^+
smooth	15	4	-	-	-	-	-	0.0498	0.553	1800	-	37
rough 2.5×	10	4	0.1032	583	0.089	2.8	22	0.0602	0.393	1500	0.74	26
rough 2.5×	15	4	0.1032	564	0.089	2.8	21	0.0582	0.581	2200	1.36	39
rough 2.5×	20	4	0.1032	573	0.089	2.8	21	0.0591	0.785	3000	2.22	52
rough 2.5×	25	4	0.1032	594	0.089	2.8	22	0.0613	0.985	3900	2.83	65
rough 15×	10	4	0.6195	114	0.089	16.8	4.2	0.0703	0.409	1900	1.99	27
rough 15×	15	4	0.6195	111	0.089	16.8	4.1	0.0688	0.601	2700	2.39	40
rough 15×	20	4	0.6195	113	0.089	16.8	4.2	0.0697	0.778	3600	2.23	52
rough 15×	25	4	0.6195	114	0.089	16.8	4.2	0.0709	0.971	4600	2.51	65

Table 2: Key flow parameters

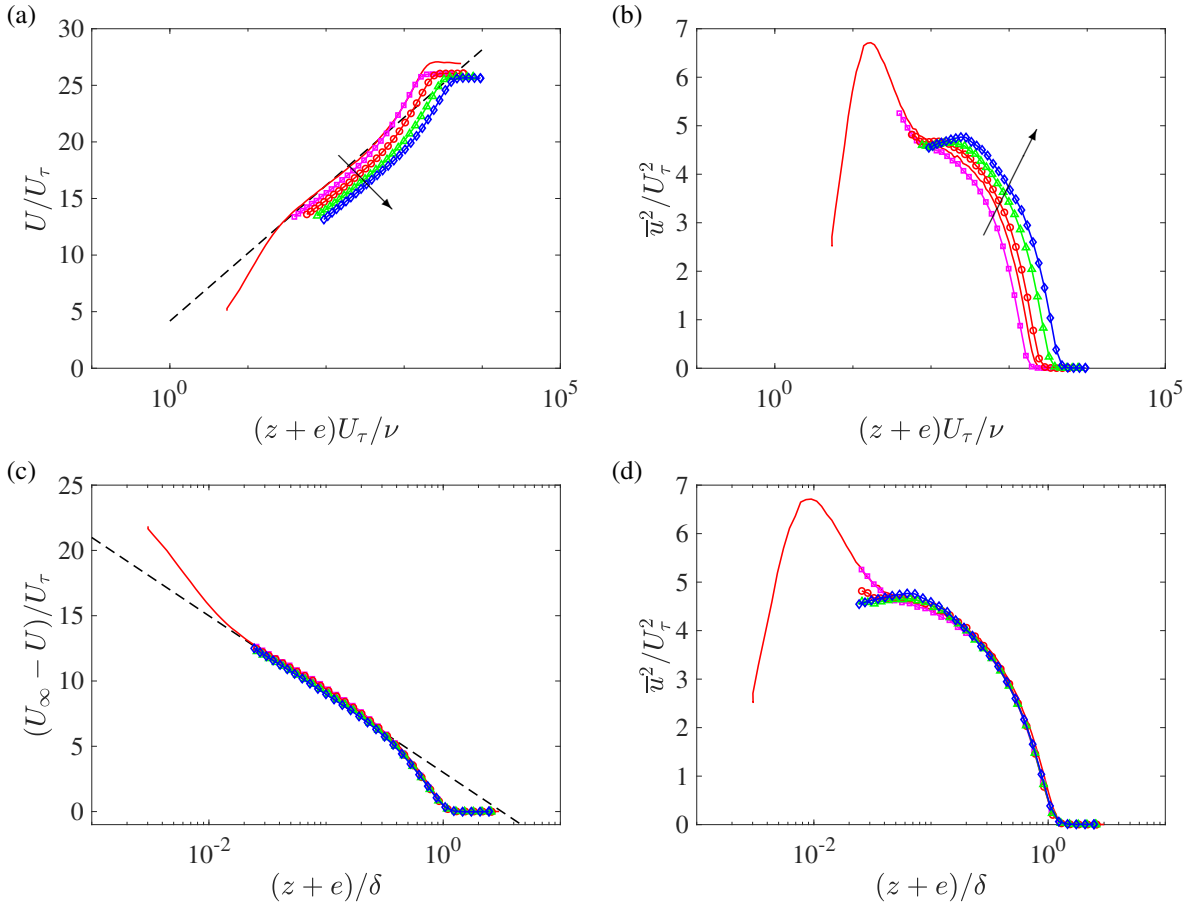

Figure 2: Mean statistics for the 2.5 times scaled roughness. Wall-normal distributions of: (a) inner scaled mean velocity; (b) inner scaled turbulence intensity; (c) mean streamwise velocity defect; (d) outer scaled turbulence intensity. Red line is smooth wall data taken at 15 m/s with $Re_\tau = 1800$. Open symbols are rough data with: square magenta, $U_\infty =$ 10 m/s, $Re_\tau = 1500$; circle red, $U_\infty = 15$ m/s, $Re_\tau = 2200$; green triangle, $U_\infty = 20$ m/s, $Re_\tau = 3000$; blue diamond, U_∞ = 25 m/s, $Re_\tau = 3900$.

tion and 21 points in the spanwise direction) covering approximately 3δ in the each direction. The skin friction velocity U_τ is estimated via forcing the rough wall measurements to collapse onto the velocity defect and outer scaled turbulence intensity of the smooth wall reference, by assuming Townsend's outer layer similarity hypothesis.

3 Results

Turbulent Flow Statistics

Figure 2 shows the wall-normal distribution of different flow statistics from the $2.5\times$ scaled roughness at several friction Reynolds number Re_τ (where $Re_\tau = \delta U_\tau/\nu$). Data are spanwise averaged over the complete measurement domain of $\approx 3\delta$, which equates to approximately 54 characteristic spanwise wavelengths of the rough surface. The skin friction velocity is estimated by forcing outer layer similarity in the velocity defect (Figure 2c) and outer scaled turbulence in-

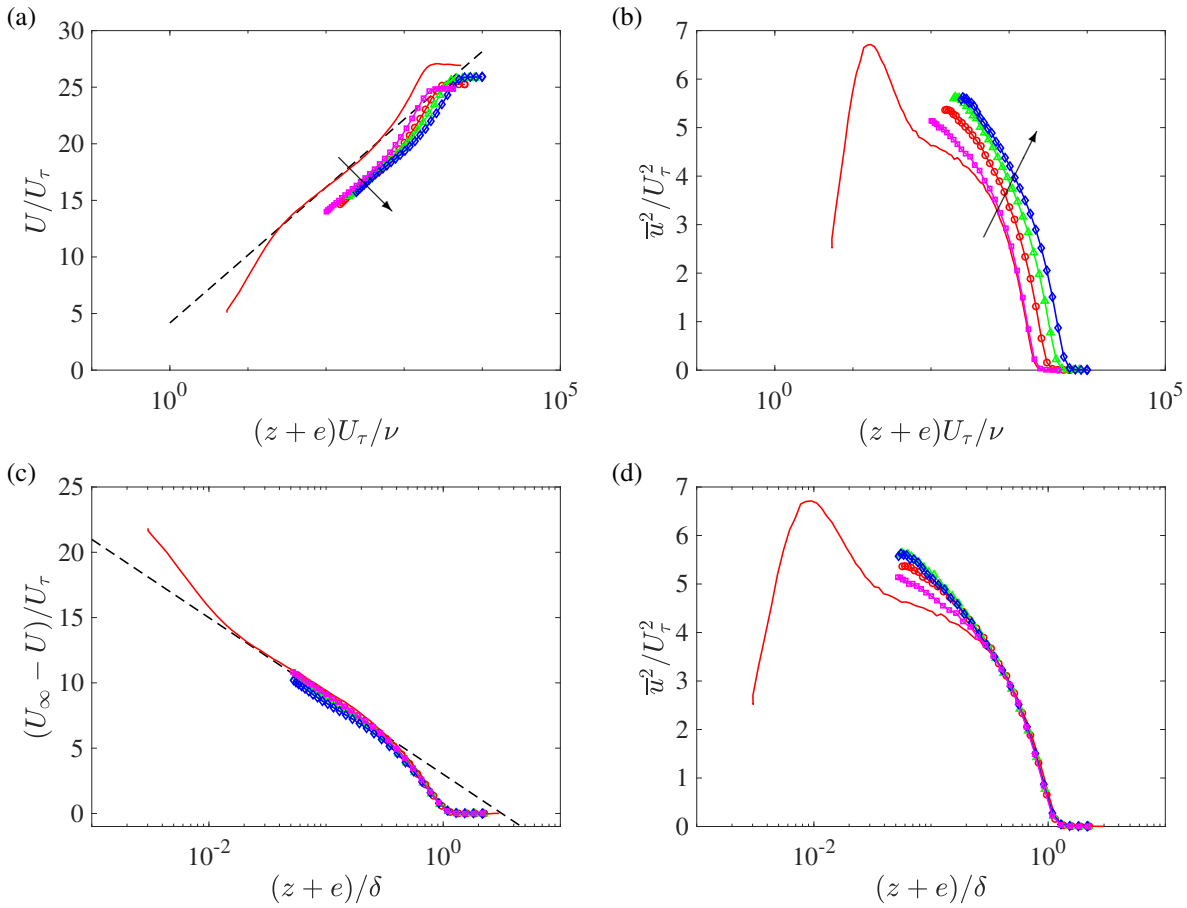

Figure 3: Mean statistics for the 15 times scaled roughness. Wall-normal distributions of: (a) inner scaled mean velocity; (b) inner scaled turbulence intensity; (c) mean streamwise velocity defect; (d) outer scaled turbulence intensity. Red line is smooth wall data taken at 15 m/s with $Re_\tau = 1800$. Open symbols are rough data with: square magenta, $U_\infty =$ 10 m/s, $Re_\tau = 1900$; circle red, $U_\infty = 15$ m/s, $Re_\tau = 2700$; green triangle, $U_\infty = 20$ m/s, $Re_\tau = 3600$; blue diamond, U_∞ = 25 m/s, $Re_\tau = 4600$.

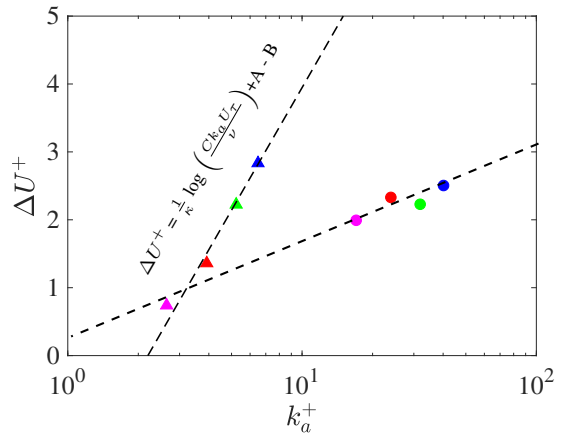

Figure 4: Velocity profile shift as a function of viscous scaled average roughness height. Closed triangle symbols show 2.5× scaled and filled circles show 15× scaled roughness

tensity (Figure 2d). Such technique has been previously used by Monty (2016). From figure 2a it is clear that the velocity profiles are increasingly shifted downwards as Reynolds number increases, which indicates the increase in skin friction drag. The inner scaled turbulence intensity about the spanwise averaged mean in figure 2b shows a clear increase in turbulent flow activity in the logarithmic region with Reynolds number. Again note that l^+ for the HWA sensor increases from 26 - 65 over the range of Reynolds numbers, and this would be expected to attenuate near-wall energy. For the highest Reynolds number (and hence highest l^+) this effect would extend up to $z^+ \approx 300$ and is visible in the variance curve of figure 2c. In general though from figure 2, we observe that the $2.5\times$ scaled roughness seems to behave like a regular isotropic-homogeneous surface roughness (see Kevin 2016 for surface roughness classification) or 'k-type' roughness (following Perry *et al.* 1969).

For the $15\times$ scaled roughness however, the results are not as straight forward. Figure 3 shows the flow statistics from the $15\times$ scaled surface roughness. Here we can see that the viscous scaled mean velocity profiles (figure 3a) do not behave like a rough surface in the classically expected manner. Though there is some initial downward shift in the mean profile for the lowest Reynolds number (see figure 3a), as Re_τ increases the profiles do not shift further downwards as would be expected for 'k-type' roughness. This is a case where

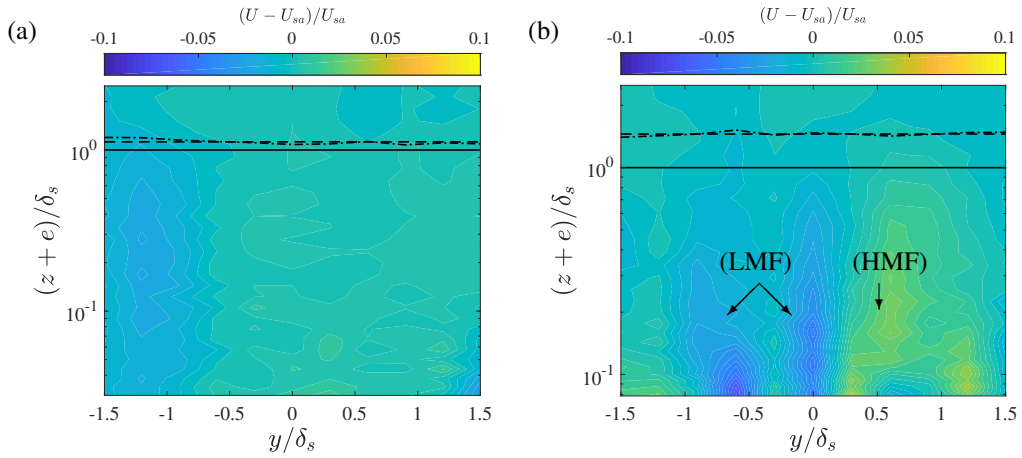

Figure 5: Spanwise variation of mean streamwise velocity U about the spanwise averaged value U_{sa} for the rough wall. Wall-normal and spanwise locations are normalised by smooth wall boundary layer thickness δ_s. (a) 2.5× scaled roughness; (b) 15× scaled roughness. Both measurements are at $x = 4$ m and $U_\infty = 15$ m/s. Dot-dashed lines represent the local boundary layer thickness over the rough, straight horizontal lines indicate the boundary layer thickness from the smooth wall reference case, and the dashed line illustrate the spanwise averaged boundary layer thickness of the rough surface. LMF indicates low momentum flow and HMF shows high momentum flow.

the roughness Reynolds number k^+ is growing, and yet the roughness function ΔU^+ seems to have almost saturated.

To view the overall effect of the two different scaled surfaces, figure 4 plots ΔU^+ against k_a^+ for the 2.5× and 15× surfaces. The figure shows that the 2.5× scaled roughness (triangle symbols) approaches a fully rough asymptote as is typically expected of k-type rough surfaces when k_s^+ is large enough, while the 15× scaled roughness (circle symbols) does not. Comparing the results from both the 2.5× and 15× scaled we see the counter-intuitive result that the smaller scaled surface behaves 'more rough' than the larger scaled one (despite the fact that the overall roughness height is 6 times smaller). Although the k_a^+ values become large for the 15× surface at the highest Reynolds numbers, and ES_x is kept constant, the 15× surface does not seem to behave like a conventional surface roughness.

The asymptotes for the 2.5× scaled roughness (triangle symbols in figure 4) follows:

$$\frac{\Delta U}{U_\tau} = \frac{1}{\kappa} ln\left(\frac{C k_a U_\tau}{\nu}\right) + A - B \qquad (1)$$

where the Kármán constant $\kappa = 0.384$, smooth wall intercept $A = 4.17$, and B = 8.5 is Nikuradse's (1933) fully rough constant. Here C is a scaling factor linking k_a to k_s, in this case $C \approx 2.4$, suggesting that the equivalent sand grain roughness for the 2.5× surface is 0.2477 mm (where k_a is 0.1032 mm). The 15× scaled roughness case however (circle symbols in figure 4), does not seem to follow this same asymptote, regardless of the value of C. For this large-scaled roughness, the ΔU^+ values also do not increase significantly with Re_τ, signalling that there is a different flow regime in this case influencing the results. Note that in spite of this behaviour, the 15× surface does have a substantially larger boundary layer thickness than the 2.5× case.

Two Dimensional Velocity Mapping

Figure 5 shows the streamwise mean velocity variation about the respective spanwise averaged rough-wall values over the complete spanwise / wall-normal measurement plane. Note that here δ_s is the boundary layer thickness over the smooth surface base case. Here figure 5(a) shows the 2.5× scaling while figure 5(b) shows the 15× scaled roughness. Both cases are measured with a freestream velocity of 15 m/s. By comparing the two cases, it is evident that the 15× scaled roughness exhibits a large scale spanwise variation (secondary flow) within the boundary layer. The variation seems to extend beyond the logarithmic region, upto $z/\delta_s \approx 0.4$, which is approximately equal to $z/\lambda = 1$.

Similar flow behaviour over heterogeneous roughness has been reported by Barros and Christensen (2014) where they observe an alternating high- and low- momentum flow over a spanwise cross-section. A more recent report by Vanderwell and Ganapathisubramani (2015) indicates that the precise form of the alternating high- and low- momentum flow depends on the roughness element spacing. They show that the secondary flow strength increases as the roughness spacing approaches δ. It seems that in our case the 15× scaled roughness, which has a characteristic spanwise lengthscale which is appreciable compared to the local boundary layer thickness $\lambda/\delta = 0.25$ ($\lambda/\delta_s = 0.34$ for scaling with smooth walled boundary layer thickness) also generates a large-scale secondary flow that influences the spanwise average mean profiles shown in figure 3a.

Discussions

From these results, it is clear that although we keep

solidity (and hence ES_x) constant, geometrically scaling a roughness to obtain larger k_a does not necessarily lead to a surface that is dynamically 'rougher'. The subtlety here that when we scale surfaces geometrically, in addition to making k larger, we also increase the in-plane wavelength of the roughness λ relative to the characteristic length scale of the turbulent boundary layer. It would appear that when this wavelength λ becomes an appreciable proportion of the boundary layer thickness, the surface ceases to behave in a 'k-type' manner.

This method of scaling roughness is commonly used to simulate or match the viscous scaled height of certain high Reynolds number engineering applications in a low Reynolds number laboratory facility. For example, to simulate the effect of biofouling on an operating ship (see Monty *et al.* 2016 for a recent example). The tentative conclusion here would be that in striving to match the viscous scaled properties in such scaled experiments, we must be cautious to avoid the regime where λ approaches δ. A more systematic investigation that involves several additional λ/δ scales and perhaps also a regular well-defined geometery (such as the egg-carton roughness explored by Chan *et al.* 2015) will be needed to provide a better understanding of this behaviour.

4 Conclusions

A study on zero pressure gradient turbulent boundary layers over a rough surface has been conducted. Here we investigated the effect of in-plane roughness wavelength, λ, with respect to the boundary layer thickness δ by geometrically scaling a simple roughness topography. The results show that the $2.5\times$ scaled roughness behaves like a typical isotropic-homogeneous surface roughness or 'k-type' roughness. The $15\times$ scaled roughness however, exhibits quite different behaviour. This surface does not approach the fully rough asymptote, and exhibits a drag penalty that is comparable or in some cases smaller than the smaller scaled surface, despite the fact that the $15\times$ scaled surface has a roughness height that is 6 times greater than the $2.5\times$ surface. This behaviour is likely associated with the fact that as the in-plane roughness lengthscale λ approaches the boundary layer thickness for the larger scaled case, secondary flows are generated. Ultimately, one might imagine that as λ became much greater than the boundary layer thickness, the boundary layer would experience the roughness in a very different sense as it rode over the undulations. This suggests that some of the odd behaviour observed for low effective slope surfaces (see Napoli *et al* 2008 and Schultz and Flack 2009) may in fact be due to a growing ratio of in-plane roughness wavelength to boundary layer thickness.

Acknowledgments

The authors would like to thank the Australian Research Council, the British Council Newton Fund, and the Australia Indonesia Center for the support of this work. B. Ganapathisubramani acknowledges support from EPSRC (Grant No: EP/P009638/1).

References

Acharya. A., Bornstein. J., and Escudier. M. P. (1986) Turbulent boundary layers on rough surfaces. *Exp. Fluids* Vol:4, 33-47.

Barros. J. M. and Christensen, K. T. (2014) Observations of turbulent secondary flows in a rough-wall boundary layers. *J. Fluid Mech.* 748, R1.

Chan. L., MacDonald. M., Chung. D., Hutchins. N., and Ooi. A., (2015) A systematic investigation of roughness height and wavelength in turbulent pipe flow in the transitionally rough regime. J. *J Fluid Mech*, Vol.771, 743-777

Flack. K. A., and Schultz. M. P., (2010) Review of hydraulic roughness scales in the fully rough regime. *J. Fluids Eng*, Vol 132, 041203.

Hama. F. R., (1954) Boundary-layer characteristics for smooth and rough surfaces. *Trans. Soc. Nav. Archit. Mar. Engrs*, Vol 62, 333-358.

Hutchins, N, Nickels, T B, Marusic, I and Chong, M. S. (2009) Hot-wire spatial resolution issues in wall-bounded turbulence. *J. Fluid Mech.* Vol:635, 103?136.

Jiménez. J., (2004) Turbulent flows over rough walls. *Annu. Rev. Fluid Mech.* Vol: 36, 173-196.

Kevin, Monty. J. P., Bai. H. L., Pathikonda. G., Nugroho. B., Baros. J. M., Christensen. K. T., and Hutchins. N. (2017) Cross-stream stereoscopic particle image velocimetry of a modified turbulent boundary layer over directional surface pattern. *J. Fluid Mech.* Vol: 813, 412-435.

Ligrani. P. M. and Bradshaw. P (1987) Spatial resolution and measurement of turbulence in the viscous sublayer using subminiature hot-wires probes. *Exp. Fluids* Vol: 5, 407-417.

Monty. J. P., Dogan. E., Hanson. R., Scardion. A. J., Ganapathisubramani. G. and Hutchins. N. (2016) An assessment of the ship drag penalty arising from light calcareous tubeworm fouling. *Biofouling* Vol 32 (4), 451-464.

Moody. L. F. (1944) Friction factors for pipe flow. *Trans ASME*, Vol 44, 671-684.

Napoli, E., Armenio, V. and De Marchis, M. (2008) The effect of the slope of irregularly distributed roughness elements on turbulent wall bounded flows. *J. Fluid Mech* Vol: 613, 385-394.

Nikuradse. J., (1933) Stromungsgesetze in rauhen rohren. VDI-Forsch 361

Nugroho. B., Hutchins. N., and Monty. J. P (2013) Large-scale spanwise periodicity in a turbulent boundary layer induced by highly ordered and directional surface roughness. *Int. J. Heat Fluid Flow* Vol: 41, 90-102

Perry. A. E., Schofield. W. H., and Joubert. P. N. (1969) Rough wall turbulent boundary layers. *J. Fluid Mech* Vol: 37, 383-413.

Schultz, M. P. and Flack, K. A. 2009 Turbulent boundary layers on a systematically varied rough wall. Phys. Fluids 21, 015104.

Townsend. A. A., (1976) The structure of turbulent shear flow, 2nd ed. Cambridge University Press.

Vanderwell, C. and Ganapathisubramani, B. (2015) Effects of spanwise spacing on large-scale secondary flows in rough-wall turbulent boundary layers. *J. Fluid Mech* 774, R2.